ADVANCED FUNCTIONAL MATERIALS
www.afm-journal.de

# Remote Magneto–Thermal Modulation of Reactive Oxygen Species Balance Enhances Tissue Regeneration In Vivo

*Giuseppina Tommasini, Susel Del Sol-Fernández, Ana Cristina Flavián-Lázaro, Anna Lewinska, Maciej Wnuk, Claudia Tortiglione, and María Moros**

**One of the hallmarks of tissue repair is the production of reactive oxygen species (ROS), which modulate processes such as cell proliferation. Although several attempts have been made to manipulate ROS levels to increase tissue repair, the lack of techniques able to remotely manipulate the redox homeostasis with spatio–temporal fashion has hindered its progress. Herein, a new approach for tuning the ROS levels using magnetic nanoparticles (MNPs) that act as nanoheaters when exposed to an alternating magnetic field is presented. Two manganese–iron oxide ($Mn_xFe_{3-x}O_4$) MNPs (with a low and a high $Mn^{2+}$ content) are designed and probed for the possibility of modulating the ROS balance by magneto–thermal stimulation in the invertebrate model organism *Hydra vulgaris*, able to fully regenerate. By evaluating the expression of selected genes involved in the maintenance of ROS homeostasis and proliferation pathways, a biphasic modulation of the ROS levels played by the MNPs is found. While MNPs with a lower $Mn^{2+}$ content are able to positively modulate the regeneration potential under magnetostimulation, MNPs with a higher $Mn^{2+}$ content cause a different redox imbalance, negatively affecting the regeneration dynamic. This innovative approach reveals a novel way of manipulating redox homeostasis that can advance in the field of tissue engineering.**

## 1. Introduction

Organisms have developed efficient response mechanisms to cope with potential injury, resulting in the initiation of complex mechanisms that lead to tissue restoration. Ineffective repair can lead to infections, inflammation, fibrotic scarring, and tissue malfunction.[1] In recent decades there has been a remarkable expansion of research on the biology of tissue repair. However, progress toward the clinical translation of effective strategies has been slower than anticipated. Several significant hurdles remain, both in the form of technical challenges and gaps in the basic understanding of the biological mechanisms of repair.

One of the hallmarks of tissue repair, both in acute and chronic wounds, is reactive oxygen species (ROS) such as hydrogen peroxide ($H_2O_2$), hydroxyl radicals ($^{\bullet}OH$), or superoxide anion ($O_2^{\bullet-}$).[2] Although high levels of ROS are associated with high intracellular stress, oxidative damage, and even cell death, low levels of ROS have a central role in redox signaling via different post-translational modifications, triggering the activation of molecular pathways involved in important processes such as cell proliferation, migration, differentiation, and angiogenesis.[3,4] More recently, studies performed in model organisms such as *Danio rerio*, *Xenopus laevis*, and *Drosophila melanogaster* demonstrated that injury-induced ROS production is also necessary for the activation of pivotal pathways such as Wnt and c-Jun N-terminal kinases (JNKs) to mediate proper fin, tadpole tail, and wing regeneration, respectively.[5–7]

Thus, a promising therapeutic approach to enhance tissue repair and/or regeneration is the possibility of manipulating the amount of intracellular ROS due to their role as secondary messengers.[2] The topical application of $H_2O_2$ on ischemic ulcers of guinea pigs improved the wound healing rate by promoting the proliferation of vascular endothelial cells.[8] However, while physiological levels of ROS are necessary for the maintenance of cell homeostasis and wound healing (oxidative eustress), excessive amounts of ROS can give rise to protein, DNA, lipid damage, delay in wound closure, and ultimately cell death (oxidative stress).[9] Despite advances in understanding the biology of wound healing and tissue repair, the possibility of successfully manipulating the redox balance for therapeutic purposes

G. Tommasini, S. D. Sol-Fernández, A. C. Flavián-Lázaro, M. Moros
Instituto de Nanociencia y Materiales de Aragón
INMA (CSIC-Universidad de Zaragoza)
C/ Pedro Cerbuna 12, Zaragoza 50009, Spain
E-mail: m.moros@csic.es

A. Lewinska, M. Wnuk
Institute of Biotechnology
College of Natural Sciences
University of Rzeszow
Pigonia 1, Rzeszow 35-310, Poland

C. Tortiglione
Istituto di Scienze Applicate e Sistemi Intelligenti "E. Caianiello"
Consiglio Nazionale delle Ricerche
Via Campi Flegrei 34, Pozzuoli 80078, Italy

M. Moros
Centro de Investigación Biomédica en Red de Bioingeniería
Biomateriales y Nanomedicina (CIBER-BBN)
Zaragoza Spain

The ORCID identification number(s) for the author(s) of this article can be found under https://doi.org/10.1002/adfm.202405282



**DOI: 10.1002/adfm.202405282**

remains a challenge. This might be a consequence of: i) the delicate balance between the ROS levels needed for maintaining physiological redox signaling (oxidative eustress) and the ROS levels needed to produce oxidative stress;[10] ii) the lack of techniques able to finely tune intracellular ROS levels and iii) the few available accurate and economic wound model systems that do not pose ethical issues.

Recently, we described the possibility of optically promoting tissue regeneration by using organic semiconducting nanoparticles (NPs) composed of poly-3-hexylthiophene (P3HT).[11] The photostimulation of human primary keratinocytes treated with P3HT NPs enhanced their migratory and proliferative behavior in a wound healing assay. In addition, in an in vivo model system, *Hydra vulgaris*, the regeneration efficiency and the stem cell proliferation were enhanced. Although the exact mechanism underlying these effects was not elucidated, significant changes in the redox balance following photostimulation were found, suggesting that an increase in ROS levels could be responsible for it.[11,12] Other options, such as photodynamic therapy and laser biostimulation to induce ROS production in situ are being explored.[13–15] Despite the promising results, the use of light to photostimulate could offer some tissue penetration limitations. Conversely, magnetic fields are safe and penetrate freely into the body, so they can be used for deep tissue stimulation.[16] In combination with magnetic nanoparticles (MNPs) they offer several advantages that can be explored for tissue regeneration.

MNP can be used as intracellular nanoheaters, producing heat with spatio–temporal control upon the application of an alternating magnetic field (AMF). This technique, known as magnetic hyperthermia (MHT), has been traditionally used to kill tumoral cells by increasing their temperature to 43–46 °C.[17] To obtain a mild MHT, the physicochemical properties of the MNPs and the AMF parameters can be tuned to achieve localized heating on the MNPs surface while maintaining the macroscopic temperature of the tissue.[18,19] As ROS can be produced when cells are subjected to elevated temperature,[20,21] the possibility of using MHT to increase ROS levels has been widely explored, especially to kill tumoral cells.[22–25] However, the use of MHT to produce low levels of ROS to increase tissue repair remains largely unexplored.

Among the models to study tissue regeneration, the freshwater polyp *Hydra vulgaris* (Cnidaria) stands out as one of the best systems due to its fascinating ability to fully regenerate. Its unique regenerative potential is active throughout adulthood and directs the creation of complete polyps from amputated body parts or from tiny pieces of excised tissue.[26,27] The unlimited proliferation, self-renewal and differentiation of stem cell lineages, cell dynamics, and tissue plasticity share striking similarities to vertebrate epithelial tissues, making *Hydra* a powerful system to study regeneration.[28] We have pioneered the use of *Hydra* as a tissue-like model system to test the thermal properties of gold and magnetic nanoparticles,[19,29–33] and to identify the underlying mechanisms, showing the usefulness of this model for the assessment of the nanoheater outcome.[19,30]

Herein, we describe the use of manganese–iron oxide ($Mn_xFe_{3-x}O_4$) MNPs to mediate intracellular heat release and promote tissue regeneration through ROS production induced by an AMF. By changing the $Mn^{2+}$ content, we could tune the heating capabilities of the MNPs and their catalytic activity, while maintaining a similar size and shape. Changes in the redox balance within the polyps were promoted by magnetostimulation and pivotal intracellular pathways related to proliferation were found modulated, opening the path to use MHT for tissue regeneration.

## 2. Results

### 2.1. Design and Characterization of Tunable Manganese Ferrite Nanoparticles

To evaluate the possibility of tuning the redox imbalance in the animals upon AMF stimulation, two MNPs based on $Mn_xFe_{3-x}O_4$ with different compositions ($x$) were obtained. The incorporation of $Mn^{2+}$ in the spinel structure can alter their effective magnetic anisotropy, saturation magnetization ($M_s$), and thus, their heating efficiency.[34] However, the heating performance of MNP also depends on the size, the size distribution, and the shape. To attempt to exclusively correlate the $Mn^{2+}$ content with the heating performance, we selected a one-step thermal decomposition method to synthesize both MNPs. This synthetic procedure allowed us to fine-tune the MNP composition by controlling the initial molar ratio between the metal acetylacetonate precursors ($Fe(acac)_3$ and $Mn(acac)_2$) (Table S1, Supporting Information). The empirical composition was determined by inductively coupled plasma optical emission spectroscopy (ICP-OES), obtaining two $Mn_xFe_{3-x}O_4$ MNPs, one with a low $Mn^{2+}$ content of $x = 0.07$ (MNP1) and one with a high $Mn^{2+}$ content of $x = 0.60$ (MNP2). The composition was confirmed by STEM-Energy-Dispersive X-ray Spectroscopy, as from the chemical map it was evident that the signal belonging to Mn ions was higher in MNP2 compared to MNP1 (Figure S1, Supporting Information). As shown in **Figure 1**a,b, the as-synthesized MNPs were very similar in size and size distribution (13 ± 2 and 14 ± 2 nm for MNP1 and MNP2, respectively) and showed a cube-like shape. Moreover, both MNPs displayed superparamagnetic (SPM) behavior at room temperature and high saturation magnetization values in the 80–85 $Am^2\ kg_{ferrite}^{-1}$ range (Figure 1c). Although the $M_s$ values were almost invariable with increasing $Mn^{2+}$ content, a slight decrease in the coercitivity ($H_c$) and remanence ($M_R$) could be observed as $Mn^{2+}$ content increased. This result suggests that both MNPs present different contributions of surface canting effects, probably due to the different distribution of cations inside the spinel structure, which in turn could directly affect $H_c$ and $M_R$ but not the net magnetic moment of the ferrite.[35] From these results, we can conclude that by tuning $Mn^{2+}$ content we can modulate the effective magnetic anisotropy ($K_{eff}$) and thus, the final magnetic response upon magnetic field exposure.

As both MNPs were obtained in organic solvents, a subsequent water transference step was required for further applications. To do so, we used a well-established polymer coating method using an amphiphilic polymer (PMAO) and thereafter we functionalized the MNPs with glucose (Glc) to improve the stability in Hydra Medium (HM).[36–38] To check the success of the functionalization steps, we measured the hydrodynamic size by dynamic light scattering (DLS) and surface charge by zeta potential (Figure S2a,b, Supporting Information). The average hydrodynamic size increased slightly after Glc addition from 23 ± 2 to 25 ± 2 nm for MNP1 and 34 ± 2 to 36 ± 1 nm for MNP2, respectively,

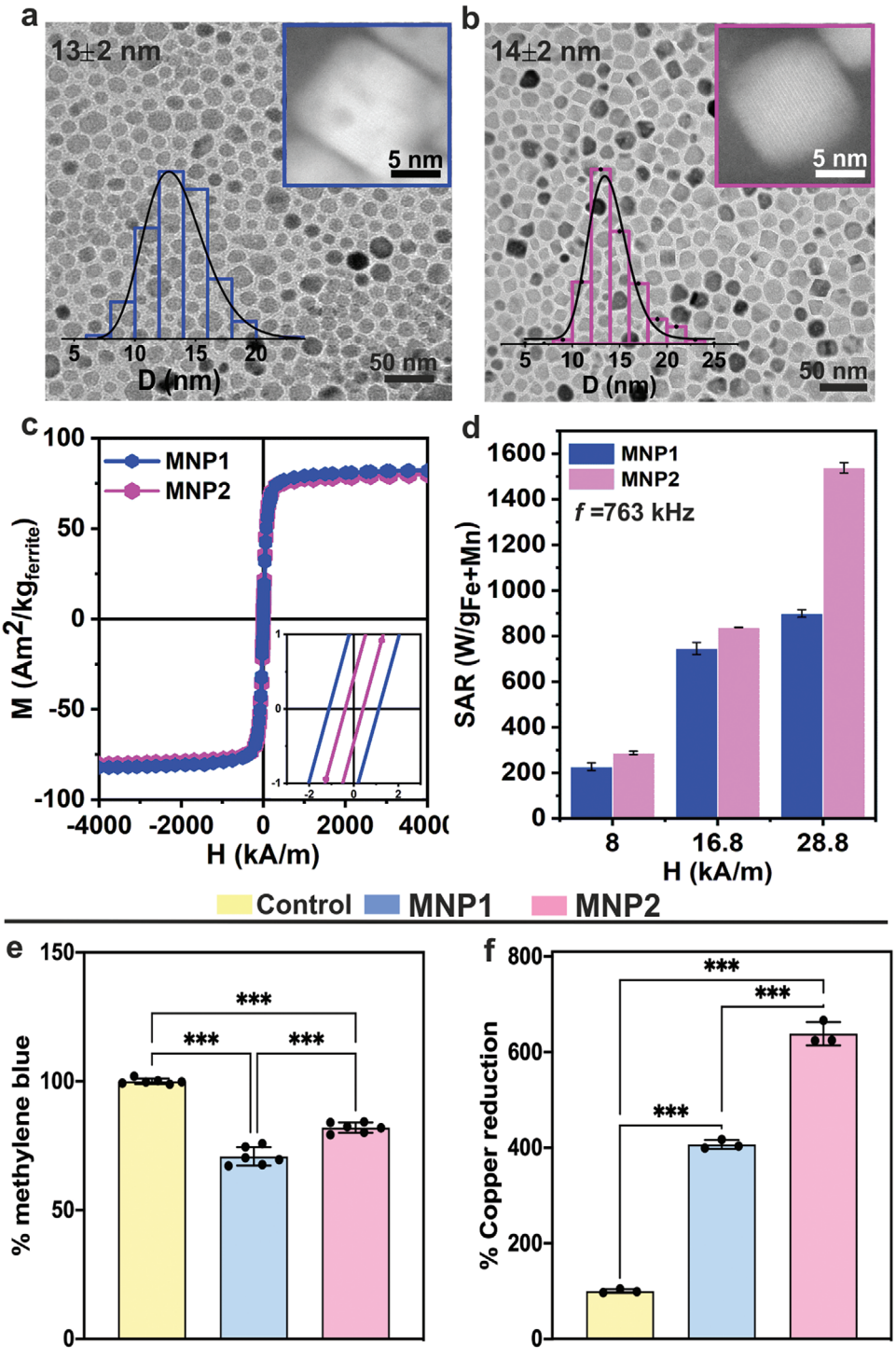


**Figure 1.** Characterization of $Mn_xFe_{3-x}O_4$ MNPs. a) Transmission electron microscopy images of as synthesized MNP1 ($Mn_{0.07}Fe_{2.93}O_4$) with average diameters of 13 ± 2 nm, and b) MNP2 ($Mn_{0.60}Fe_{2.40}O_4$) with diameters of 14 ± 2 nm. Insert: Size distributions of each MNP and its high-resolution transmission electron microscopy (HRTEM) showing their cubic-like shape and crystallinity. c) Hysteresis curve comparison of the MNPs measured at room temperature. d) SAR values obtained using a fixed frequency (763 kHz) and different field strengths (8–28.8 kA $m^{-1}$) in water. e) Methylene blue degradation assay to measure Fenton-like catalytic activity of both MNP. f) BCA assay measuring the reduction of $Cu^{2+}$ to $Cu^{1+}$ by MNP. Data is shown as the mean ± SEM of two independent experimental replicas. Statistical comparisons were performed using one-way ANOVA followed by Tukey's post hoc test (***$p < 0.001$).

whereas the zeta potential became less negative (from −44 ± 2 to −32 ± 2 mV for MNP1 and −32 ± 1 to −29 ± 1 mV for MNP2 respectively). This indicates that the functionalization with Glc was successful. The latest was also confirmed by agarose gel electrophoresis where a reduction of the electrophoretic mobility was detected after the addition of Glc (Figure S2c, Supporting Information).

To elucidate if the content of $Mn^{2+}$ had an impact on the heating capacity of the MNPs coated with PMAO under an AMF, we studied the heat production by MNP1 or MNP2 (1 $mg_{Fe+Mn}$ $mL^{-1}$) upon exposition to different AMF strengths (8 up to 28.8 kA $m^{-1}$) and a fixed frequency of 763 kHz (Figure 1d). As expected, the heating capability in terms of specific absorption rate (SAR) displayed a linear increase with the strength of the applied AMF due to the SPM behavior of both MNPs. Under the same conditions (H = 28.8 kA $m^{-1}$ and $f$ = 763 kHz) MNP2 could increase the temperature of water more than MNP1 (Figure S3, Supporting Information), resulting also in the highest SAR value in all tested conditions. For further experiments, we selected the AMF conditions (H = 28.8 kA $m^{-1}$ and $f$ = 763 kHz) where our MNP produced the greatest amount of heat.

### 2.2. Catalytic Activity of the MNP

Next, we attempt to demonstrate if the MNP could have a different catalytic activity using two semiquantitative approaches, the methylene blue and the bicinchoninic acid (BCA) assay.

Mn ferrite MNPs can act as Fenton catalysts and decompose $H_2O_2$ under neutral and physiological conditions, leading to the formation of highly reactive hydroxyl radicals which can react with methylene blue.[39] The catalytic degradation of the methylene blue was evaluated using $H_2O_2$ as an oxidizing agent. As shown in Figure 1e, MNP1 displayed a significant degradation of methylene blue on the order of 30% compared to the 18% impaired by MNP2. This indicates a higher decomposition of $H_2O_2$ by MNP1, probably due to their higher content of Fe ions compared to MNP2,[40,41] and it is in accordance with other works where the highest content of ROS was generated by the MNP with the highest content of Fe.[42] On the other side, we evaluated the redox activity of the MNPs using the BCA assay, which is based on the reduction of $Cu^{2+}$ to $Cu^{1+}$ catalyzed by MNP (Figure 1f). In this case, MNP2 displayed a higher $Cu^{2+}$ reduction capacity than MNP1, which can be related to the amount of $Mn^{2+}$ or a difference in the PMAO coating density, as also suggested by thermogravimetric analysis (Figure S4, Supporting Information).[43] MNPs with a high ability to reduce $Cu^{2+}$ have been related to a higher ROS production inside cells, finally resulting in mitochondrial reprogramming and a lack of proliferation.[43]

### 2.3. Toxicology and Uptake of Manganese Ferrite Nanoparticles

*Hydra* is known to be highly sensitive to many toxicants and can rapidly respond in the presence of them, displaying a wide range of morphological aberrations.[44] We checked the biocompatibility of the MNPs in whole animals at different levels, namely the morphological state and the reproduction rate. The toxicological impact of MNPs was tested by treating living animals with increasing doses of MNPs functionalized with Glc (ranging from 0.5 mg of Fe $mL^{-1}$ up to 2 mg of Fe $mL^{-1}$) and quantifying the morphological changes induced, according to a well-established method (Figure S5a, Supporting Information).[45,46] Upon 24 h treatment, animals did not show any signs of morphological changes such as contracted body, swelling or disintegrated tentacle, or tissue damages, indicating the absence of macroscopic toxicity induced by either MNPs, even at the highest dose tested (Figure S5b,c, Supporting Information).

On the other hand, under favorable conditions, *Hydra* polyps normally reproduce asexually through a controlled budding process. Population growth rate assessment is considered a reliable toxicity endpoint as environmental factors such as toxic agents, temperature changes, or food availability greatly affect *Hydra* population reproduction.[44,47] Adult polyps asexually active were incubated with the lowest dose of MNPs (0.5 mg of Fe $mL^{-1}$), and the number of emerging buds and newly spawned polyps was daily monitored over 10 days (Figure S6a, Supporting Information). The growth curves (Figure S6b, Supporting Information) showed no impact of MNPs per se on the *Hydra* reproduction rate.

To evaluate the uptake and MNPs internalization in *Hydra* tissue, polyps were treated with MNPs functionalized with a fluorophore (TAMRA) at 0.5 mg of Fe $mL^{-1}$. *Hydra* has a rather simple anatomy with a hollow tubular shape only composed of two cell layers, and its body transparency allows in vivo tracking and biodistribution studies of fluorescent molecules and compounds.

Imaging of treated polyps either living or fixed, showed a strong fluorescent signal homogeneously spotted all over the tentacles and the body, mainly localized in the ectodermal cell layer (**Figure 2a**) and profoundly different from autofluorescence of untreated polyps. The presence of granular fluorescent spots suggests that MNPs were internalized and accumulated into storage granules, as already reported for other inorganic NPs.[19,48–49] In addition, elemental analysis by ICP-OES showed that internalized iron increased as the incubation dose increased (Figure 2b). Both MNPs showed similar iron incorporation (i.e., 15 ng of Fe/polyp for MNP1 compared to 12.5 ng of Fe/polyp for MNP2 when incubated with 0.5 mg of Fe $mL^{-1}$), which was expected due to their similar size, shape, and coating. The iron content was higher compared to that reported for smaller and spherical MNPs coated with the same polymer (1.46 ng of Fe/polyp),[19] reinforcing the idea that the size and shape of the MNPs are critical factors driving the internalization rate.

Overall, our results indicate that both MNPs were internalized into *Hydra* tissue and did not produce adverse effects at the whole animal level even at the highest tested concentration after 24 h of incubation.

### 2.4. MNPs with Different $Mn^{2+}$ Content Mediate Different Redox Imbalances in Whole Intact Polyps

To test if we could promote a redox imbalance after magneto–thermal stimulation we used in the first instance whole polyps instead of regenerating stumps to avoid interferences from ROS produced by the wound per sè.[50] To this end, we analyzed by real-time quantitative reverse transcription PCR (qRT-PCR) the

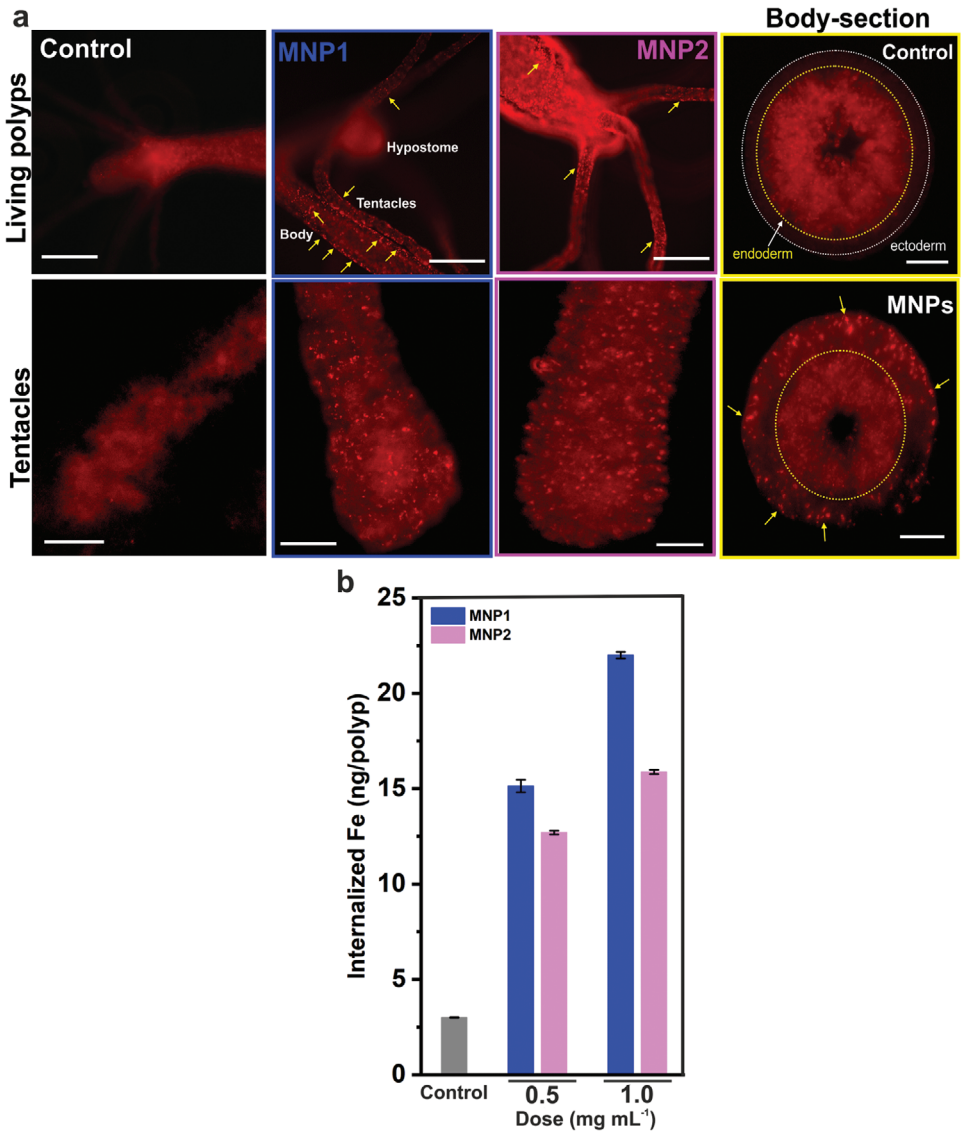


**Figure 2.** Internalization of manganese ferrite nanoparticle in *H. vulgaris* tissues. a) Fluorescence microscopy images of untreated polyps or polyps treated with MNP1 and MNP2 previously modified with the fluorophore TAMRA. Images of living polyps are present in the upper row and tentacles from fixed animals are in the lower row. Right panel: body insert. Ectoderm (white) and inner endoderm (yellow) of polyps. A control polyp is shown in the upper row and an MNP-treated polyp in the lower row. MNP (granular fluorescent spots) are indicated with a yellow arrow. Scale bar: 500 µm (living polyps) and 50 µm (tentacles and body section). b) Amount of Fe per animal determined by ICP-OES after soaking the animals with different doses of both types of MNPs overnight.

expression profile of selected genes involved in the antioxidant response, namely cytoplasmatic superoxide dismutase (*SOD1*), catalase (*CAT*) and forkhead box O (*FoxO*) and the general stress response, i.e., heat shock protein 70 (*Hsp70*) in polyps treated with MNPs and exposed to 30 min of AMF. SOD1 (cytosol) and SOD2 (mitochondria) can convert superoxide ($O_2^{\bullet-}$) into $H_2O_2$ and $O_2$, avoiding its accumulation and potential damage to proteins and lipids. Thereafter CAT is implicated in the decomposition of $H_2O_2$ into water and molecular oxygen (**Figure** 3a).

Immediately after AMF exposure only polyps treated with MNP2 showed an upregulation of *Hsp70* transcript levels, suggesting a specific effect for this MNP in the absence of any stimulation (Figure 3b). The intracellular increase of temperature generated by the local heating of MNP1 or MNP2 mediated by AMF was not able to modulate *Hsp70* expression at the analyzed time point, correlating with previous results where the overexpression was only observed 120 min post-treatment.[19]

The analysis of antioxidant enzyme gene expression also revealed different inputs elicited on the intracellular ROS balance depending on the MNP used. Unexpectedly, treatment with MNP2 but not with MNP1 per sé produced a twofold increase in the *SOD1* transcript levels, further increasing after AMF exposition; this might be related to the high production of superoxide anion ($O_2^{\bullet-}$) (Figure 3c). An increase in *CAT* levels was also induced by treatment with MNP2 in the absence of AMF,

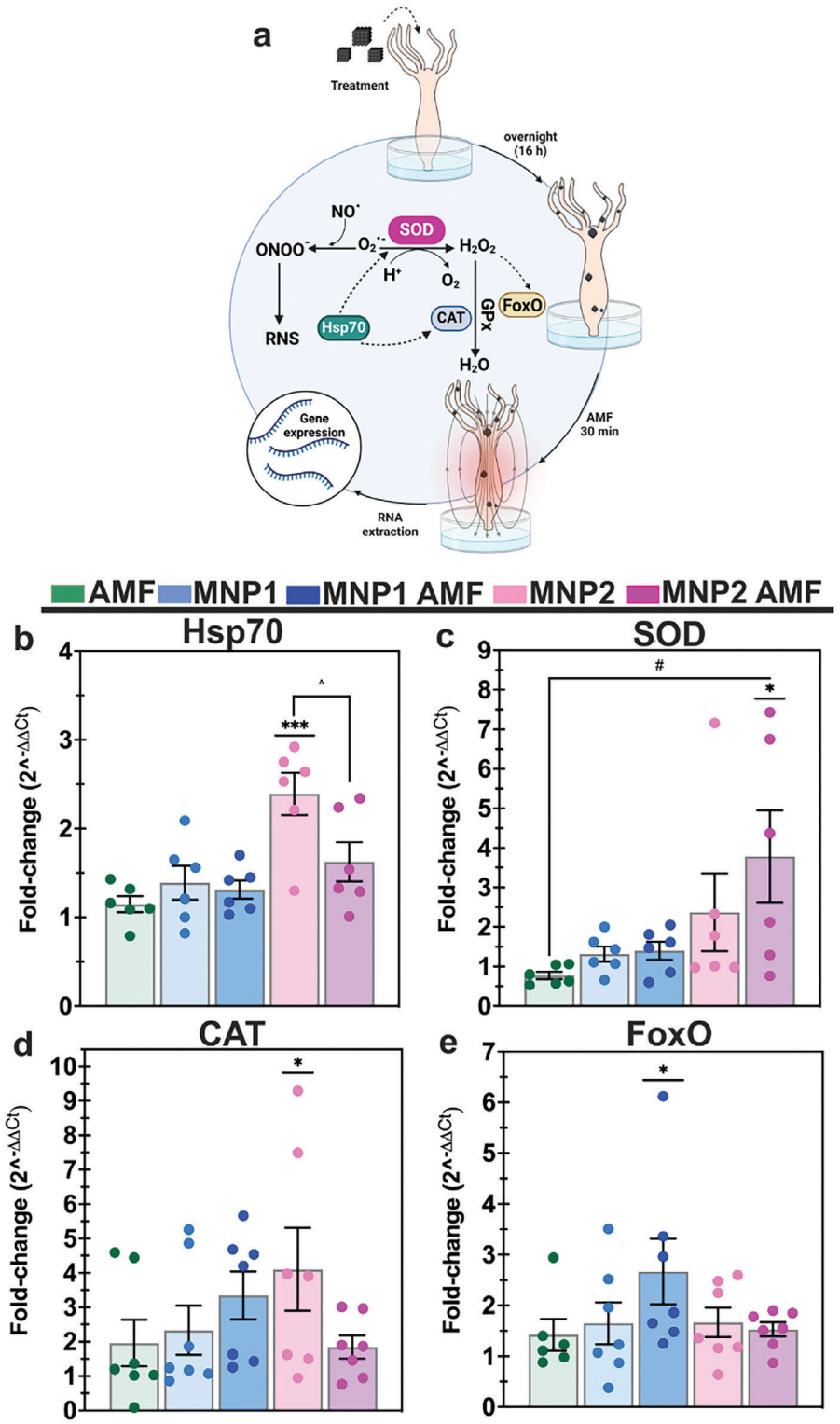


**Figure 3.** Expression profile of selected genes involved in antioxidant response and general stress. a) Diagram showing the experimental workflow and the general antioxidant defense mechanism of the animals. SOD can convert superoxide ($O_2^{\bullet -}$) into $H_2O_2$ and $O_2$, while CAT is implicated in the decomposition of $H_2O_2$ into water and molecular oxygen. b–e) qRT-PCR gene expression of b) *Hsp70*; c) *SOD1*; d) *CAT*; and e) *FoxO* involved in antioxidant and general stress. Genes were analyzed after treating polyps with 0.5 mg of Fe $mL^{-1}$ of MNPs overnight and applying 30 min of AMF (763 kHz, 28.8 kA $m^{-1}$). Results are shown as fold change mean ± SEM of three independent biological replicas, and data were normalized using elongation factor 1$\alpha$ (*Ef1α*) as a reference gene. Black asterisks (*) show samples with normalized fold expression statistically different from untreated controls. All other symbols refer to samples statistically different from those compared within branches: hash (#) refers to control AMF versus MNPs AMF; circumflex (^) refers to comparison between MNPs (either with AMF or without AMF treatment). Statistical analysis was performed using ordinary one-way ANOVA followed by Tukey's post-hoc test. (*$p < 0.05$; ***$p < 0.001$).

and with MNP1+AMF, suggesting the generation of intracellular $H_2O_2$ concentrations in these samples (Figure 3d).

As in other animals, oxidative and heat stress can activate in *Hydra* the transcription factor *FoxO* and start a molecular program leading to increased levels of antioxidant enzymes to restore homeostasis.[51,52] As shown in Figure 3e, we found an upregulation of *FoxO* gene expression specifically in polyps treated with MNP1+AMF, suggesting the triggering of different molecular targets for MNP1 and MNP2. Interestingly, both in humans[53] and in *Hydra FoxO* is also responsible for the proliferation and continuous self-renewal of stem cells.[54]

As increased ROS levels mediated by both MNPs may stimulate the synthesis of non-enzymatic and enzymatic antioxidants to maintain the redox balance, two parameters to estimate the total antioxidant activity were then evaluated, i.e., the total antioxidant capacity (TAC) test (FRAP assay in an acidic environment measuring the activity of non-thiol antioxidants) and the analysis of thiol levels (reduced glutathione (GSH) content). Even if elevated levels of TAC and thiols were found for both MNPs compared to untreated polyps, once again the impact of both MNPs was not the same. MNP2, presenting the highest content in $Mn^{2+}$, had a greater contribution to the thiol levels response, whereas the effect of MNP1 was more evident in promoting non-thiol antioxidant activity (Figure S7, Supporting Information).

In summary, magneto–thermal stimulation of MNP1 acted preferentially at the *CAT* level, suggesting higher levels of $H_2O_2$, while MNP2 + AMF modulated *SOD1* levels, more related to superoxide anion ($O_2^{\bullet-}$) production.[55]

### 2.5. MNPs with the Lowest $Mn^{2+}$ Content Boost Regeneration In Vivo Upon AMF Exposure

The redox imbalance observed in whole polyps confirmed the MNPs' potential to modulate the intracellular redox signaling. We then investigated the effect of AMF-stimulated MNPs on *Hydra* regeneration, by evaluating the dynamic and the efficiency of the head regrowth after decapitation. Treated and untreated animals were bisected at subhypostomal level (80% of body column length) and stimulated with an AMF twice a day (**Figure 4a**). The head regeneration efficiency was evaluated by morphometric analysis assigning a numerical score to each developmental stage: *stage 0* indicates wound closure; *stage 1*, where tentacles start to appear; *stage 2*, where tentacles reach 2/3 of the final length; and finally, *stage 3*, complete tentacles regrowth (Figure 4a). Regenerating stumps were monitored using an optical microscope, and developmental stages were quantified at regular intervals post-amputation (h p.a.), obtaining the distribution percentage under different treatments (Figure 4b,c).

Comparing the developmental distributions with untreated animals, no significant differences were observed for polyps treated with AMF (untreated AMF) or MNP1 alone (MNP1), indicating that neither the AMF nor the treatment with MNP1 had an impact on the regeneration efficiency rate. On the contrary, polyps treated with MNP1 and exposed to AMF (MNP1+AMF) showed a clear enhancement of regeneration efficiency already at 30 hp.a (Figure S8, Supporting Information) with 28% of polyps at *stage 1* (purple bar) compared to the 10% obtained in untreated animals. The differences were more accentuated at 48 hp.a where animals treated with MNP1+AMF showed a significant boost in the regeneration efficacy, with 18% of the polyps having a complete head and tentacle regrowth (*stage 3*—red bars) compared with 5% for the untreated polyps (Figure 4c). A completely different outcome was observed during *Hydra* regeneration when using MNP2, as a large number of stumps (≈66%) were still in the earliest developmental stages (*stage 0*—light purple bars) at 48 hp.a, denoting a striking inhibitory effect played by the MNP2 per sè. The application of AMF (MNP2 +AMF) did not have an improved effect on animal regeneration, even when these MNPs had better heating capabilities than MNP1.

To decipher the molecular mechanism underlying the response triggered by MNPs and MHT treatment, we then explored by qRT-PCR selected genes from the Wnt/*β*-catenin signaling pathway, which plays a key role throughout the entire process of *Hydra* head regeneration.[56–58] As different members of the canonical Wnt signaling, such as Wnt ligands, Sp5, Dishevelled, and *β*-catenin, are activated early during head regeneration,[58,59] we evaluated the expression of *Wnt3, Sp5, β-catenin* at 5 and 24 hp.a. (Figure 4d). Our data showed an increase in the levels of *Sp5* and *β-catenin* transcripts at 5 hp.a. when both MNPs were magnetostimulated (Figure 4f,g). Although higher levels of *β-catenin* transcripts could be expected in the sample with the fastest regeneration rate (MNP1+AMF), not only the transcript levels are important, as *β-catenin* should also translocate into the nucleus and interact with Tcf/Lef in order to activate downstream target genes.[60] Thus, an absence in the stabilization of *β-catenin* could also be responsible for impairing the regeneration rate, even when *β-catenin* transcript levels are maintained.[61]

Similar to vertebrates, in *Hydra Wnt3* acts as a positive regulator of the regeneration process, and in regenerating polyps the higher levels occur at 12 and 48 h p.a.[62] While no differences in the transcript levels of *Wnt3* were observed at 5 h p.a. (Figure 4e), there was a significant upregulation for MNP1+AMF samples at 24 h p.a. when compared to 5 h p.a. ones. Conversely, we could not observe an upregulation of *Wnt3* in samples treated with MNP2 (with or without AMF) even at 24 h p.a., which is in accordance with the lack of regeneration enhancement observed. We have previously reported that the decrease of *Wnt3* levels could explain the absence of an enhancement of *Hydra* regeneration when using P3HT and photostimulation, while upregulation of *Wnt3* could be related to an increase in the regeneration process.[11] The different regulation of *Sp5* and *Wnt3* in MNP1 + AMF observed at 5 h p.a. could be attributed to the temporal dynamic of the two genes,[63] and we cannot exclude the possibility that the time window used in our experiments precluded us from observing an earlier *Wnt3* upregulation induced by MHT treatment.

In conclusion, while only slight differences in the expression levels were observed for *β-catenin* and *Sp5* due to the high endogenous levels of these transcripts at 5 h p.a., at 24 h p.a. clear differences were observed for *Wnt3* levels between MNP1+AMF and MNP2+AMF. Altogether, these data support, at least in part, the implication of the Wnt/*β*-catenin pathway in the different

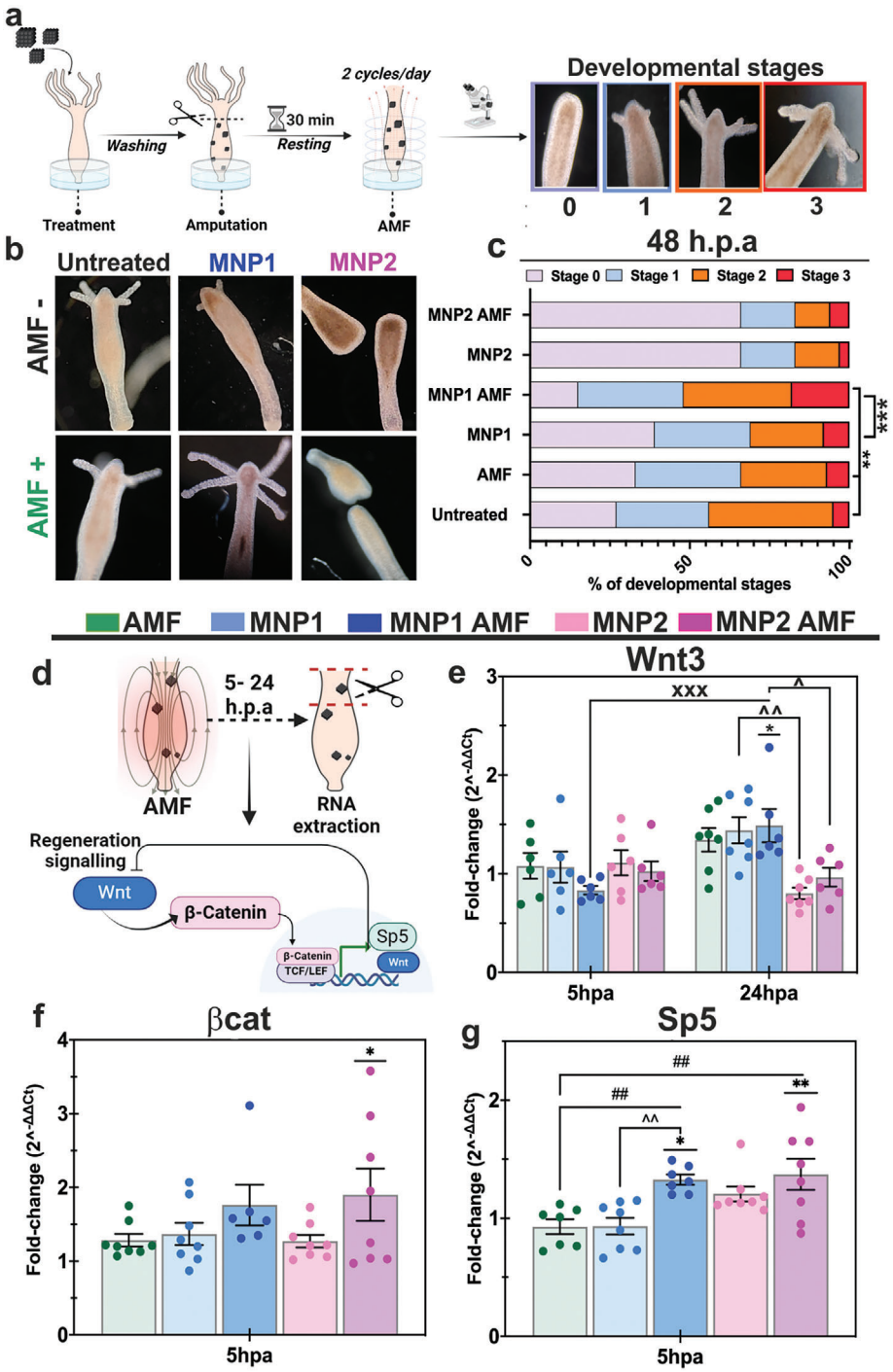


**Figure 4.** Impact of magnetic hyperthermia on *H. vulgaris* regeneration capacity. a) Schematic diagram showing the experimental workflow and the classification of developmental stages of regenerating heads. b) Representative images of animals treated with MNP1 or MNP2 and bisected before applying (or not) the AMF after 48 h p.a. c) Quantitative distribution of developmental stages at 48 h p.a. from three independent biological replicates (N, is the total number of animals per condition, $N_{Untreated} = 60$; $N_{AMF} = 63$; $N_{MNP1} = 64$; $N_{MNP1+AMF} = 66$; $N_{MNP2} = 71$; $N_{MNP2+AMF} = 66$). Statistical comparisons were performed using the Chi-square test ($\chi^2$ and p values for each comparison listed in Table S2, Supporting Information). (** $p < 0.01$; *** $p < 0.001$). d) Diagram showing the experimental workflow and molecular interplay between genes implied in the Wnt/$\beta$-catenin signaling. e–g) qRT-PCR expression profiles of selected genes involved in the regeneration process using as internal control elongation factor 1$\alpha$ (*Ef1α*). e) *Wnt3*; f) *β-catenin*; g) *Sp5*. Results are shown as fold change mean ± SEM of three independent biological replicates. Black asterisks (*) show samples with normalized fold expression statistically different from untreated controls. All other symbols refer to conditions statistically different from those compared with branches: hash (#) refers to control AMF versus MNPs AMF; circumflex (^) refers to the comparison between MNPs (either with AMF or without AMF treatment); cross (×) refers to 5 h versus 24 h. Statistical comparisons were performed using ordinary two-way ANOVA followed by Bonferroni post hoc test e) or one-way ANOVA followed by Tukey's post hoc test f, g) (*$p < 0.05$; **$p < 0.01$; ***$p < 0.001$).

regeneration outcomes between groups. However, this signal is highly complex and we cannot rule out that other important pathways, such as *Hippo/Yap*, that act synergically in promoting and stabilizing the body axis during head regeneration could be involved.[64]

### 2.6. Magneto–Thermal Stimulation Modifies the Intracellular Redox State of Regenerating Polyps

While the modulation of the Wnt pathway is involved in the regeneration, the mechanism implied in its activation after injury is not completely understood. In *Hydra*, it has been recently reported that $Ca^{2+}$ release and ROS molecules act as first messengers triggering the injury response, and thus are essential to start the tissue regeneration program.[65,66] Based on this evidence, we wondered if the acceleration of the dynamic of the head regeneration elicited by MNP1+AMF was also based on a ROS-mediated mechanism. Direct measurement of ROS production in the whole animal using standard fluorescent probes is difficult due to the body thickness and the polyp autofluorescence. To assess in a semi-direct way the generation of ROS in regenerating animals we used Amplex UltraRed reagent, an assay widely used for $H_2O_2$ detection from biological samples.[65] The assay is based on the horseradish peroxidase-catalyzed oxidation of Amplex Red to resorufin in the presence of $H_2O_2$ (**Figure 5a**). MNP2 per se produced a higher signal than MNP1, and in both cases, AMF application increased it. However, magnetostimulation of MNP2 resulted in higher ROS production from the beginning. This will be a direct evidence that AMF application increases ROS levels in amputated animals and that both MNPs behave differently in terms of ROS production.

To corroborate this data and obtain further information, we studied the antioxidant response in an indirect way, selecting 5 h p.a. and 24 h p.a. as the time points to perform RNA and protein extraction of regenerating polyps. This would partially avoid the interference of the ROS generated by the wound. First, we evaluated the expression of antioxidant genes, like *SOD1, SOD3, CAT*, and glutathione peroxidase (*GPx*).[65] At the analyzed time window (5 h p.a.), expression levels analyzed by qRT-PCR of *SOD1, SOD3*, and *CAT* were not modulated for MNP1 or MNP1+AMF, which could be consistent with an earlier expression during the regeneration (Figure 5b–d; Figure S9a, Supporting information). Indeed, CAT activity measured at the protein level (5 h p.a.) was higher for MNP1 + AMF treated polyps (Figure 5f), indicating a fast response in return to the higher levels of $H_2O_2$ produced after MHT. Unexpectedly, *SOD1* and *SOD3* were downregulated in polyps treated with MNP2 and MNP2+AMF, suggesting the presence of low levels of superoxide anion (Figure 5b,c). Since in whole polyps, the MNP2+AMF treatment suggested opposite results (Figure 3c), we cannot exclude the possibility that in regenerating polyps superoxide anion was produced and then transformed into other reactive species, such as Reactive Nitrogen Species (RNS).[67] Low levels of superoxide anion and SOD could finally result in low levels of $H_2O_2$ with a consequent downregulation of *CAT* expression levels for MNP2+AMF at 24 h p.a. (Figure 5d).

Although both MNPs could affect TAC and thiol levels, MNP1+AMF had a greater contribution to the non-thiol antioxidant activity (Figure S9b, Supporting Information), mirroring what happened in intact polyps (Figure S7, Supporting Information). On the contrary, MNP2+AMF polyps presented the highest levels of thiol content (GSH, measured at the protein level) (Figure 5g), correlating with the highest overexpression of *GPx* (Figure 5e). As GPx/GSH are implied in the removal of radical forms of ROS but also of RNS,[68] the hypothesis of RNS production by MNP2+AMF could be supported.

To lastly confirm that increased ROS production upon combined treatment with MNPs + AMF had an adaptive hormetic effect and no detrimental effect such as oxidative damage to biomolecules, the analysis of lipid peroxidation was then considered. No lipid peroxidation was observed upon MNPs + AMF treatment as judged by no changes in the content of malondialdehyde, one of the end products of lipid peroxidation (Figure S10, Supporting Information), indicating that MNPs + AMF-mediated ROS production is not sufficient to promote oxidative damage and related adverse effects. MNP-treated animals in the presence of the AMF were protected against ROS-induced lipid peroxidation by elevated levels of *GPx* and glutathione. Indeed, the members of the glutathione peroxidases family can reduce free $H_2O_2$ to water and lipid hydroperoxides to their corresponding alcohols using GSH as a cofactor.

### 2.7. Mitogen-Activated Protein Kinases Modulation After Magnetostimulation

Recently a link between mitogen-activated protein kinases (MAPK) and Wnt pathways during regeneration has been proposed in *Hydra*.[66] MAPK signaling (ERK, p38, and JNK) is essential for triggering Wnt signaling in *Hydra* head regeneration, its activation occurring in response to ROS and $Ca^{2+}$ signaling promoted after injury.[66] Similarly, in *Drosophila* JNK signaling in injured tissues is needed to activate the Wnt pathway to trigger regeneration of the wing.[7]

Therefore, we analyzed whether SAPK/JNK and ERK signaling were also involved in the different outcomes in regeneration caused by both MNPs. To do that, polyps were treated (or not) with MNPs, bisected, and exposed to an AMF for 30 min, before analyzing the protein lysates.[66]

As shown in **Figure 6a**, $pERK^{T202:Y204}$ protein levels were increased in all samples when compared to untreated polyps, except in the case of MNP2+AMF, where a strong inhibition of this pathway was observed. On the contrary, levels of the phosphorylated JNK (pJNK) relative to tubulin were similar between all groups (Figure 6b). Overall our data suggest that the different redox imbalances caused by MNP1+AMF and MNP2+AMF could finally affect the MAPK signaling, which is ultimately related to the modulation of *Wnt/β-catenin* pathway.

## 3. Discussion and Conclusion

Herein, we have demonstrated the possibility of increasing tissue regeneration by manipulating the redox homeostasis, using MNP and MHT. While the idea of increasing wound healing by manipulating ROS levels is well known,[2,8] the lack of traditional

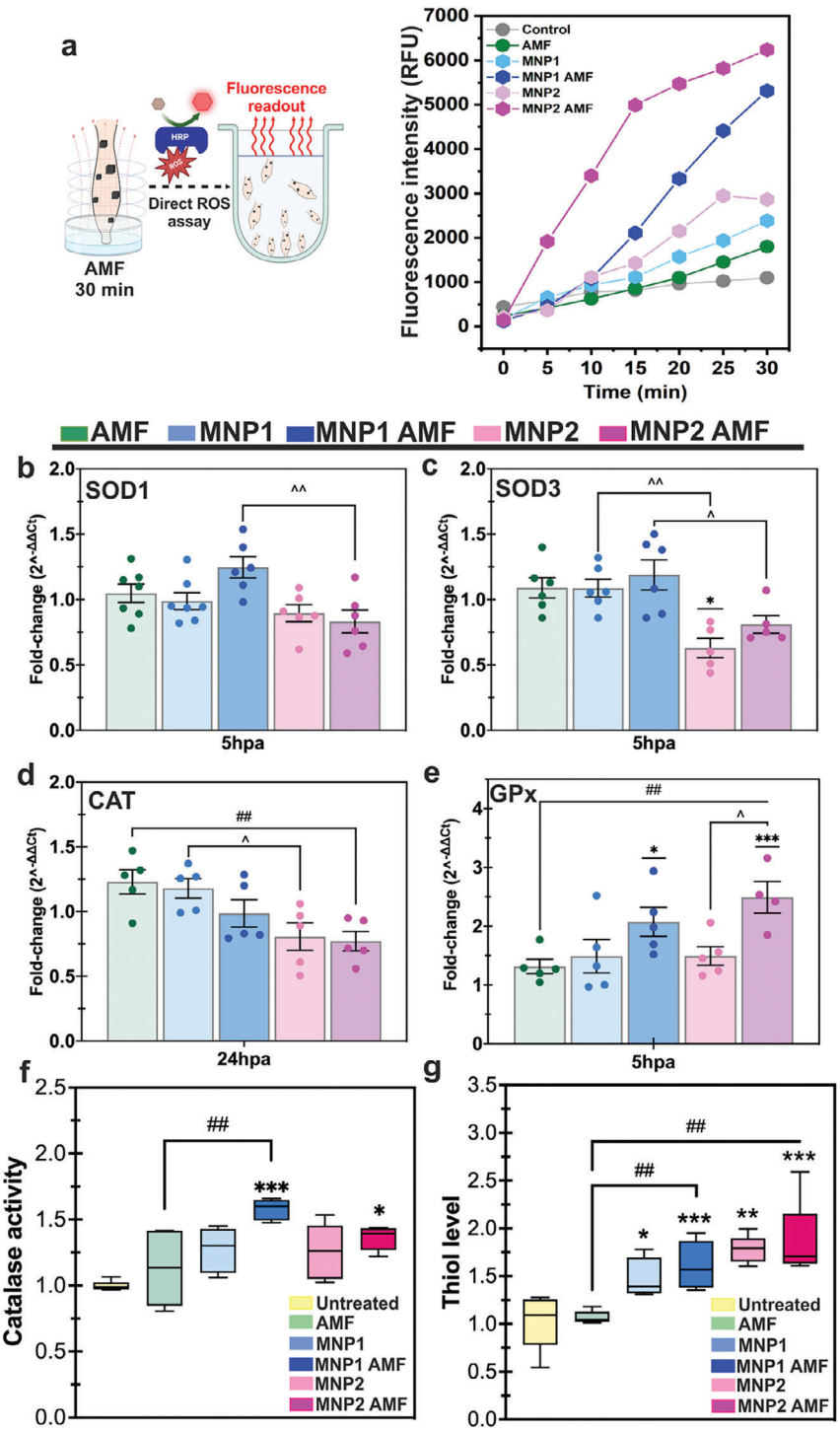


**Figure 5.** Evaluation of the redox imbalance caused by the MNPs and the AMF in regenerant animals. a) Schematic representation of Amplex Ultra-Red assay used to quantify $H_2O_2$ and/or $OONO^-$ levels in regenerating polyps treated with MNPs, bisected and exposed to an AMF. 30 min p.a. they were transferred into a well containing Amplex Red and the changes in the fluorescence intensities were recorded during time. b–e) Expression profile of genes involved in the antioxidant defense using as internal control the elongation factor 1$\alpha$ (*Ef1α*). b) *SOD1*; c) *SOD3*; d) *CAT*; e) *GPx*. Results are shown as fold change mean ± SEM from three independent biological replicates. f) CAT activity and g) thiol levels measured using protein extracts obtained 5 h p.a. Data are normalized using untreated polyps as control condition ($n = 6$ from two independent biological replicates); the interquartile range represents the 25th to 75th percentiles while the horizontal line in the middle of the box represents the median value. Whiskers represent 5–95% CI. For all graphs, black asterisks (*) represent samples statistically different from untreated controls. All other symbols refer to samples statistically different from those compared between branches: hash (#) refers to control AMF versus MNPs AMF; circumflex (^) refers to comparison between MNPs (either with AMF or without AMF treatment). Statistical comparisons were performed using ordinary one-way ANOVA followed by Tukey's post hoc test (*$p < 0.05$; **$p < 0.01$; ***$p < 0.001$).

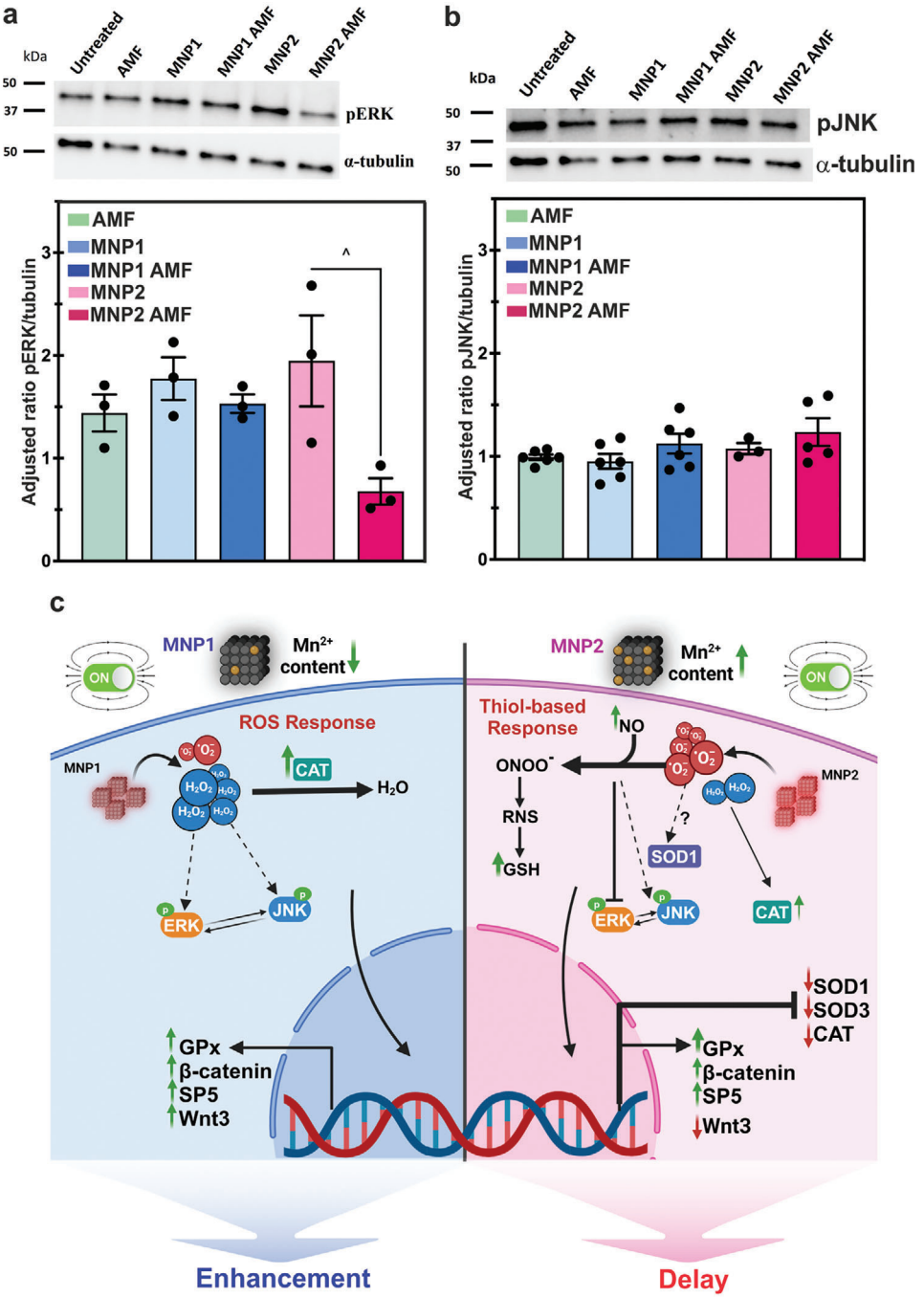


**Figure 6.** Modulation of MAPK signaling in regenerating animals mediated by MHT and MNPs. a, b) Representative Western blots of phosphorylated $ERK^{T202:Y204}$ and $SAPK/JNK^{T183:Y185}$ from regenerating animal lysates. Quantification of pERK bands and $pJNK^{T183:Y185}$ relative to $\alpha$-tubulin loading control. c) Proposed models of the biological pathways implied in the regeneration process mediated by MNP1 (left) and MNP2 (right) upon AMF application in *Hydra vulgaris*. Figure created with BioRender.com. Statistical comparisons were performed using ordinary one-way ANOVA followed by Tukey's post hoc test ($^*p < 0.05$).

approaches to finely tune them has hampered its advancement.[9] Recently, the use of photodynamic therapy or light is being explored to induce ROS in a more controlled fashion,[11,13–15] but the limited penetration of light in thick tissues can be a problem.[69] On the contrary, the use of magnetic fields offers different advantages, such as the possibility to penetrate deep into the body and to generate local heat in a spatial and temporal fashion when used in combination with MNP. Heat is known to play a major role in different biological processes such as osteogenesis, angiogenesis, or nerve regeneration,[70,71] and it is also implicated in the generation of ROS, which has been traditionally explored to kill tumoral cells.[24] While the reason behind this enhanced production is still

unclear, a hypothesis could be that the increased temperature in proximity to the MNP might boost the kinetics of the Fenton-like reaction.[72,73] By tuning the $Mn^{2+}$ content we synthesized two MNPs with different heating capabilities and catalytic activity, while size, size distribution, and shape were maintained. While it is widely accepted that MNP can have a peroxidase-like activity, a definitive statement about the generation of ROS is difficult to obtain due to the differences in the MNP design and experimental settings reported.[24] Our results demonstrated a biphasic modulation of the oxidative stress played by both MNPs. MNPs with the lower $Mn^{2+}$ content were able to boost the regeneration potential under magnetostimulation, sustained by a significant increase over the analyzed temporal window in the transcript expression levels of genes related to the Wnt pathway (*Wnt3*). Conversely, MNPs with a higher $Mn^{2+}$ content (MNP2) negatively affected the regeneration dynamic, which correlated with an inhibition in the *Wnt3* levels. As the size, coating, and internalization rate between both MNPs were similar, we excluded them as the main factors driving the different outcomes.[74] While the composition of the MNPs can affect ROS production,[42] different ions leaking from both MNPs and/or the generation of other reactive species, such as RNS, cannot be excluded.

Even when the exact mechanism occurring during the regeneration process with both MNPs is difficult to fully address, we speculate that the observed differences are caused by a different redox imbalance, that in the case of MNP1 +AMF is also associated with a ROS-mediated tissue regeneration. The results from the Amplex Red assay (Figure 5a) are direct evidence that the application of the AMF increased the production of ROS in the amputated animals compared with MNPs alone and that MNP2+AMF produced higher levels of ROS. Aside from this assay, in regenerating animals the clearest differences between both MNPs were found at the antioxidant enzyme transcript levels, with *SOD1, SOD3,* and *CAT* downregulated for animals treated with MNP2 and MNP2+AMF. Superoxide anion can react with the nitric oxide free radical ($NO^{\bullet}$) to form the RNS peroxynitrite ($ONOO^{-}$) at a constant rate higher than that of the dismutation of superoxide by SOD.[75] As $NO^{\bullet}$ production is increased during *Hydra* regeneration,[76] we hypothesize that this increase in $NO^{\bullet}$ levels, together with a higher increase of superoxide anion caused by MNP2, led to a faster formation of $ONOO^{-}$, downregulating SOD and CAT. This hypothesis is supported by the fact that not only hydrogen peroxide but also $ONOO^{-}$ can oxidize Amplex Red and thus be detected in this assay.[77,78] In this case, the upregulation of *GPx* and GSH levels found in animals treated with MNP2 and MNP2+AMF could be a measure to remove the excess of RNS radicals (Figure 6c).[79,80]

On the other hand, the higher activity of CAT imposed by MNP1+AMF suggested that similar to what happened in whole animals, a higher concentration of $H_2O_2$ was formed. These data are consistent with the higher regeneration rate observed for this sample, as $H_2O_2$ is less reactive, and thus it is considered a better candidate to activate signaling pathways than other ROS species such as hydroxyl radical ($OH^{\bullet}$) or superoxide anion ($O_2^{\bullet -}$).[55]

Lastly, the differences between both MNPs were also observed in the balance of the MAPK signaling cascade, with MNP2+AMF inhibiting the phosphorylation of ERK, while MNP1+AMF did not have a big impact neither in JNK or ERK. However, this signaling is highly complex, as ERK and stress-induced MAPKs (p38 and JNK) can display an antagonist effect, being JNK anti-apoptotic while ERK displays a pro-apoptotic function.[66] Although further studies are needed to specifically dissect the exact actors that are implied, our results open the path to the increase of tissue repair by modulating the redox homeostasis using magneto–thermal stimulation, an alternative not explored before. Furthermore, the biphasic modulation of ROS balance caused by the two MNPs lays the groundwork for the use of different MNPs to control the activation of different pathways.

## 4. Experimental Section

*Materials*: Iron (III) acetylacetonate ($Fe(acac)_3$, 97%), manganese (II) acetylacetonate ($Mn(acac)_2$, 98%), oleic acid (OA, 90%), 1,2-hexadecanediol (technical grade, 90%), dibenzyl-ether (DBE, 90%), and poly(maleic anhydride-alt-1-octadecene) (PMAO) (MW = 30 000–50 000 Da), N-(3-dimethylaminopropyl)-N-ethylcarbodiimide hydrochloride (EDC) and 4-aminophenyl $\beta$-D-glucopyranoside were purchased from Sigma–Aldrich. Tetramethylrhodamine 5-(and -6)-carboxamide cadaverine, (TAMRA) was purchased from Anaspec. All solvents were of analytical grade and used as received.

*Synthesis of Manganese Iron Oxide Nanoparticles by One-Step Thermal Decomposition Method*: Two systems based on $Mn_xFe_{3-x}O_4$ MNPs were synthesized by the thermal decomposition method according to a procedure previously described by Sun with slight modifications.[81] In brief, for MNP1 synthesis 13 mmol of $Fe(acac)_3$, 2 mmol of $Mn(acac)_2$, 40 mmol of oleic acid as surfactant, and 30 mmol of 1,2-hexadecanediol were used in 150 mL of benzyl ether. Meanwhile, to produce MNP2 3.33 mmol of $Fe(acac)_3$, 1.67 mmol of $Mn(acac)_2$, 45 mmol of oleic acid, and 30 mmol of 1,2-hexadecanediol were employed in 50 mL of benzyl ether. For both approaches, the mixture was mechanically stirred (100 rpm) under a flow of $N_2$ and then heated up to 200 °C for 2 h (5 °C $min^{-1}$), afterward heated to 285 °C (3 °C $min^{-1}$) for another 2 h. The black–brown mixture was cooled to room temperature by removing the heat source. Under ambient conditions, ethanol excess was added to the mixture, and a black material was precipitated and separated using a permanent magnet. The black product was dissolved in hexane and precipitated again with ethanol. This cycle was repeated three times, giving a dark brown powder, which was dispersed in hexane and kept at 4 °C.

*Transference to Water with PMAO Polymer and Dye Functionalization*: The transference into water was performed following a previously reported method with slight modifications.[36,37] In brief, 225 mg of poly(maleic anhydride-alt-1-octadecene) (PMAO) was added to a flask containing 195 mL of chloroform ($CHCl_3$) and placed in an ultrasonic bath for 30 min at room temperature. Subsequently, 10 mg of Fe $mL^{-1}$ of MNPs in 5 mL of $CHCl_3$ were added dropwise, and the mixture was sonicated for another 30 min. Afterward, the solvent was slowly removed under vacuum (200 mbr, 40 °C) using a roto-evaporator. MNPs were then resuspended in basified water (20 mL of NaOH 0.05 M) and rotavaped (200 mbr, 70 °C) until complete evaporation of chloroform. At this point, the solution became clear as MNPs were completely transferred into the water. To remove the excess of unbound polymer the MNPs solution was centrifuged at 24 000 rpm for 2 h four times.

TAMRA-labeled MNPs were obtained using the same procedure but previously modifying 1% of the PMAO monomers with a fluorescent dye (TAMRA) under magnetic stirring overnight in chloroform.[36]

*Functionalization with Glucose*: Functionalization with glucose was performed by incubating 1 mg Fe of MNPs with 15.6 µmol of N-(3-dimethylaminopropyl)-N′-ethylcarbodiimide hydrochloride (EDC), 25 µmol of 4-aminophenyl $\beta$-D-glucopyranoside in 250 µL of SSB buffer pH 9 (boric acid 50 mM and sodium borate 50 mM). After 3 h of incubation at room temperature, the ligand excess was removed by washing the MNPs with phosphate-buffered saline (PBS 1X) pH 7.4 in a centrifugal filter with a membrane of 100 kDa molecular weight limit (Merck Millipore, Darmstadt, Germany) four times. Finally, the MNPs functionalized with glucose were stored at 4 °C for further use.

*Characterization of the MNPs and their catalytic activity*: The MNPs' size and shape were evaluated by TEM using a Tecnai T20 microscope (FEI, Netherlands) working at an acceleration voltage of 200 kV. TEM samples were prepared by depositing 5 µL of dilute solution on a copper grid (200 mesh) and drying it at RT prior to analysis. MNPs size distributions were obtained by measuring more than 200 NPs with the Image J software. The elemental analysis was performed using an inductively coupled plasma optical emission spectrometry (ICP-OES) instrument (PERKIN ELMER mod. OPTIMA 2100 DV). Typically, 25 µL of a $Mn_xFe_{3-x}O_4$ MNPs suspension were digested in 1 mL of Aqua Regia (3:1 HCl:$HNO_3$) at 60 °C overnight and diluted upto a volume of 25 mL with deionized water. The samples were measured in triplicates. The hydrodynamic diameters of MNPs and zeta potential were measured using dynamic light scattering measurements (Nanosizer ZS, Malvern, UK) at 25 °C. For the magnetic characterization, the MNP suspensions were lyophilized and measured as powder, put into gelatine capsules, and immobilized with cotton wool. Hysteresis loops were measured using a superconducting quantum interference device (SQUID, from Quantum Design) magnetometer at 300 K fields up to 4000 kA $m^{-1}$. The magnetic hyperthermia measurements of the MNPs were performed in a Nanoscale Biomagnetics D5 series device. The CAL 2 coilset composed of an open glass dewar flask with a rotary vacuum pump was used. The temperature change was measured with an optic fiber sensor incorporated into the equipment (measurement range −40–200 °C). Thermal measurements of MNPs in water were performed at 1 mg of Fe $mL^{-1}$ under a fixed frequency of 763 kHz and different intensities (3.8, 8, 16.8, and 28.8 kA $m^{-1}$) of AMF for 300 s. The SAR values were obtained with the initial linear slope method using the first 30 s of the heating curves.

To assess the catalytic activity of the MNPs, two semi-quantitative assays were performed. The methylene blue degradation assay was performed to determine the amount of ROS generated from the surface of the nanoparticles, following a previously reported protocol.[22] Samples were prepared using methylene blue 5 µg $mL^{-1}$, MNPs 75 µg $mL^{-1}$, and 30% $H_2O_2$ 245 mM in 1 mL of Hydra medium. As a control, Hydra medium was mixed with methylene blue and 30% $H_2O_2$ at the aforementioned concentrations. The samples were incubated at RT for 30 min and centrifuged for 45 min at 14 500 rpm. 200 µL were transferred into a 96-multiwell plate, and the absorbance was measured at 665 nm using a Synergy H1 microplate reader (BioTek). To assess the redox capacity of the MNPs, BCA assay was performed in accordance with a previously reported protocol.[82] 200 µL of BCA reagent was mixed with 200 µL of MNPs at a concentration of 0,5 mg $mL^{-1}$. As a control, 200 µL BCA reagent was mixed with 200 µL of water. The samples were incubated for 2 h at 37 °C, then centrifuged for 5 min at 10 000 rpm in a centrifugal filter with a membrane of 100 kDa molecular weight limit (Merck Millipore, Darmstadt, Germany). 300 µL were transferred into a 96-multiwell plate and the absorbance at 570 nm was measured using a Synergy H1 microplate reader (BioTek). The absorbance of the control was assigned to 100% and the absorbance of the samples was converted to percentage taking into account the reference of this value.

*Animal Culturing*: *Hydra vulgaris* (strain Zurich) was asexually cultured in Hydra Medium (HM: 1 mM $CaCl_2$ and 0.1 mM $NaHCO_3$, pH 7) according to the method of Loomis and Lenhoof.[83] Polyps were kept at 18 °C with a 12:12 h light: dark regime and fed thrice a week with freshly hatched *Artemia salina* nauplii. For all the experiments, polyps starved for at least 12 h were selected from a homogeneous population. *Hydra vulgaris* culturing and handling do not require ethical approval from national authorities.

*Toxicological Evaluation—Morphological Analysis*: To evaluate the MNPs biocompatibility, groups of ten polyps were soaked for 24 h with culture medium supplemented with increasing doses of MNPs modified with glucose (ranging from 0.5 up to 2 mg of Fe $mL^{-1}$) in a 24-multiwell plate at 18 °C. After treatment, polyps were washed in HM and morphological alterations were monitored and quantified in vivo by using a stereomicroscope (SZX7 Olympus) equipped with a digital color camera.[46,84] Untreated polyps soaked in bathing HM were used as controls.

*Toxicological Evaluation—Hydra Asexual Growth Rate*: In a typical assay to estimate the asexual growth rate of *Hydra* polyps, groups of six founder polyps per condition were treated with 0.5 mg of Fe $mL^{-1}$ overnight with both MNPs-Glc, then washed and placed in a 24-well plate (1 animal per well) to individually follow their growth rate. Untreated polyps at the same developmental stage were used as controls. Founder polyps with at least one bud were selected and all animals were fed once daily for 10 days. The growth rate constant (k) of an exponentially growing group of animals was determined according to Bosch and David.[85] k was determined from $\ln(n/n_0) = kt$, where n is the number of animals per day (t) and $n_0$ is the number of founder animals at $t_0$. Three independent experiments were performed for each growth rate curve.

*Uptake of MNPs in Whole Animals*: The internalization and uptake of MNP-Glc were evaluated using two different approaches described below:

Fluorescence Microscopy: To evaluate MNPs internalization, groups of five polyps per condition were treated as described above with TAMRA-labelled MNPs (0.5 mg of Fe $mL^{-1}$). Prior to imaging, polyps were briefly relaxed in 2% urethane in HM and fixed in paraformaldehyde 4% for 2 h at room temperature. The presence of internalized MNPs was evaluated by fluorescence microscopy (Nikon Eclipse Ti-E, Amsterdam, The Netherlands) and images were acquired with the software Nikon NIS-Element.

Inductively Coupled Plasma Optical Emission Spectroscopy (ICP-OES): The amount of iron uptaken per polyp was further measured by ICP-OES spectroscopy analysis. 100 polyps were treated for 24 h with two different doses of MNPs-Glc (0.5 or 1 mg of Fe $mL^{-1}$) at 18 °C. Polyps were then abundantly washed and sample digestion was performed at 90 °C for 1 h with $HNO_3$. After resting overnight at room temperature, digested samples were diluted in MilliQ water prior to ICP-OES analysis.

*Magnetic Hyperthermia Treatment in Regenerating Polyps*: To evaluate the effect of MHT on *Hydra* regeneration rate, groups of 20 polyps were placed into a 24-multiwell plate and incubated overnight with 0.5 mg of Fe $mL^{-1}$ of MNP1-Glc or MNP2-Glc in HM to a final volume of 400 µL. Afterward, polyps were washed and decapitated using a scalpel to perform a sub-hypostomal cut (80% body length). Amputated polyps were then collected in glass vials of 2 mL and exposed in staggered order 30 min per cycle to an AMF ($f$ = 763 kHz, 28.8 kA $m^{-1}$), finding no signs of adverse effects either macroscopically or by TUNEL assay (data not shown). Throughout the magnetic stimulation, temperature changes in polyps medium were measured with an optic fiber sensor Neoptix T1, finding in all cases a maximum increase of 4 °C. To be sure that all experiments were performed in controlled temperature conditions, control animals (AMF-) were always incubated in a water bath at the same global temperature. In a typical MHT assay, two cycles per day of magneto–thermal stimulation were performed, 5 h separated from each other. Regenerative stages were monitored using a stereomicroscope (SZX7, Olympus) and quantified at different time points (24, 30, 48, and 72 h) post-amputation (h p.a.). The efficiency of regeneration was evaluated by comparing the percentage distribution of regenerative stages for each experimental condition. Untreated polyps, whether exposed to AMF or not, were used as controls.

*qRT-PCR Analysis in Whole and Regenerating Animals*: Expression profiling of selected genes in whole polyps or regenerating animals exposed to MHT treatment was performed using qRT-PCR using the following protocols.

For whole animals, 15 polyps per condition were treated overnight with MNP1-Glc or MNP2-Glc (0.5 mg of Fe $mL^{-1}$) in HM. After treatment, polyps were abundantly washed with HM and one cycle of MHT was performed as described above (763 kHz, 28.8 kA $m^{-1}$ for 30 min). RNA was extracted at 0 h (immediately after AMF application) from treated and untreated polyps. Similarly, for regenerating animals, 20 polyps per condition were treated overnight with both MNPs-Glc (0.5 mg of Fe $mL^{-1}$). After treatment, polyps were abundantly washed with HM and head amputation was performed (sub-hypostomal cut). Decapitated polyps were exposed to 2 or 3 cycles of AMF (763 kHz, 28.8 kA $m^{-1}$) and RNA was extracted from wound tips at 5 h and 24 h p.a. from treated and untreated polyps. For both analyses, total RNA extraction was performed using the Total RNA Extraction Kit (Norgen Biotek, Corp.) following the manufacturer's instructions, and its concentration was determined by

absorbance using Synergy H1 microplate reader (BioTek). First-strand cDNA synthesis was obtained using the High-Capacity cDNA Reverse Transcription Kit (Applied Biosystem), following the manufacturer's instructions, and qRT-PCR was performed using iTaq Universal SYBR Green Supermix (Bio-Rad) in a CFX Opus 96 Real-Time PCR System (Bio-Rad). For qRT-PCR amplification, the following cycling steps were used: initial denaturation for 30 s at 95 °C, followed by 40 cycles at 95 °C for 5 s, 58 °C for 30 s. In addition, melting curves (from 60 to 95 °C, increment 0.5 °C) were generated to check any undesired amplification products. HyEf1$\alpha$ was used as a reference gene and relative expression levels were calculated using the delta–delta Ct ($2^{-\Delta\Delta CT}$) method.[86] Specific primers for *Hydra* genes amplification were designed using the Primer3 software (http://frodo.wi.mit.edu/primer3/) and NCBI primer-BLAST tool (https://www.ncbi.nlm.nih.gov/tools/primer-blast/) (Table S3, Supporting Information). Three independent biological replicates for each gene and condition were carried out.

*Direct Detection of ROS in Regenerating Polyps*[65]: The Amplex UltraRed (ThermoFisher Scientific, A36006) solution containing 100 µM Amplex UltraRed and 0.2 U $mL^{-1}$ of Horseradish peroxidase (HRP) was freshly prepared prior to each assay. Ten animals per condition were treated overnight with 0.5 mg of Fe $mL^{-1}$ of MNP1-Glc or MNP2-Glc in HM. After treatment, polyps were washed with HM and head amputation was performed. Decapitated polyps were exposed to 1 AMF exposition (763 kHz, 28.8 kA $m^{-1}$) for 30 min and immediately transferred with 50 µL of HM into a 96-well microplate, with each well pre-filled with 50 µL of Amplex UltraRed solution. The fluorescence intensities were recorded in a Synergy H1 microplate reader (BioTek) for 30 min in 5 min increments with an excitation/emission maxima 490/585 nm. The background value obtained by measuring a well containing 50 µL of Amplex UltraRed solution diluted in 50 µL HM, was subtracted from each result.

*Biochemical Assays on Whole and Regenerating Polyps*: For all biochemical assays, a group of 20 polyps was treated following the same protocols reported above (see Magnetic hyperthermia treatment in regenerating polyps and qRT-PCR analysis in whole and regenerating animals in the Experimental Section). Whole polyps were collected after applying the first cycle of MHT. Regenerating polyps were collected at 6 h p.a. in Eppendorf tubes and homogenized to obtain a tissue extract that was analyzed with different biochemical approaches below:

Total Antioxidant Capacity (TAC): Total antioxidant capacity was determined in homogenized *Hydra* cell extracts using the ferric reducing antioxidant power (FRAP) assay as described previously.[30] Briefly, the reduction of $Fe^{3+}$-TPTZ (iron[III]-2,4,6-tripyridyl-S-triazine) to $Fe^{2+}$-TPTZ by compounds with potential antioxidant activity in *Hydra* samples was assessed in an acidic environment as judged by an increase of absorbance at 593 nm using an absorbance microplate reader. TAC was calculated as Trolox equivalent antioxidant capacity (TEAC) and the results were normalized to samples taken from untreated control animals.

Levels of Free Thiols Measurement: Thiol levels were determined in homogenized *Hydra* cell extracts using ThiolTracker Violet Dye as a measure of the content of reduced glutathione (GSH) (T10096, Thermo Fisher Scientific, Waltham, MA, USA). Briefly, the staining protocol was applied according to the manufacturer's instructions and the fluorescence was measured using a fluorescence microplate reader and excitation/emission maxima of 404 and 526 nm, respectively. The fluorescence results in fluorescence relative units (RFU) were normalized to samples taken from untreated control animals.

Catalase Activity: Catalase activity in homogenized *Hydra* cell extracts was measured using Catalase Assay Kit (CAT100, Merck KGaA, Darmstadt, Germany). Briefly, the colorimetric assay was performed according to the manufacturer's instructions and after color development, the absorbance was read at 520 nm using an absorbance microplate spectrophotometer. The results were normalized to samples taken from untreated control animals.

Lipid Peroxidation Assay: Lipid peroxidation was evaluated in homogenized *Hydra* extracts using Lipid Peroxidation Assay Kit (MAK085, Merck KGaA, Darmstadt, Germany) as described previously.[11] Briefly, lipid peroxidation was determined by the reaction of malondialdehyde (MDA) with thiobarbituric acid (TBA) to form a fluorometric ($\lambda_{Ex} = 532/\lambda_{Em} = 553$ nm) product, proportional to the content of MDA. The fluorescence results in fluorescence relative units (RFU) were normalized to samples taken from untreated control animals.

*Western Blot and Quantitative Analysis of Mitogen-Activated Protein Kinases (MAPK) in Regenerating Polyps*: To evaluate the activation of the MAPK (pJNK and pERK) cascade in *Hydra* regenerating polyps after MHT treatment, a group of ten polyps were treated following the same protocol already described under the head "Magnetic hyperthermia treatment in regenerating polyps" in the Experimental Section. Polyps were exposed to one AMF cycle and lysates were obtained 45 min p.a. using RIPA buffer (Sigma–Aldrich). Protein concentration was quantified by absorbance using the Micro BCA assay kit (Thermo Fisher), according to the manufacturer's instructions. 5 µg of protein per lane was mixed with 4X loading buffer (SDS 4X, 5% v/v 2-mercaptoethanol), boiled 5 min at 95 °C and separated by SDS-PAGE using pre-casted gels (4–15% Mini-PROTEAN TGX Gels, Bio-Rad). Proteins were then blotted on 0.2 µm nitrocellulose membranes (Trans-Blot Turbo Transfer Pack, Bio-Rad) using a Trans-Blot Turbo system (Bio-Rad) and selecting the 1.5 mm gel protocol (10 min, 1.3A and 25 V). After blotting, membranes were blocked with 5% BSA in TBS-T (Tween 0.1%) for 2 h and incubated at 4 °C with primary antibodies diluted 1:1000 in 1% BSA in TBST. The day after, membranes were washed in TBS-T (three times, 10 min each) and incubated with HRP-conjugated secondary antibody diluted 1:2000 in 1% BSA in TBS-T for 2 h at RT. Membranes were then washed in TBS-T (four times, 10 min each one) and bands were detected applying a 1:1 mix of enhanced chemiluminescent reagent (SuperSignal West Femto Maximum Sensitivity Substrate, Thermo-Fisher) using a ChemiDoc Imaging System (Bio-Rad). To evaluate loading controls, the same membranes were incubated in a mild stripping solution (1.5% w/v glycine, 0.1% w/v SDS, 1% v/v Tween 20, pH 2.2) for 10 min at 37 °C and then another 20 min at room temperature. After stripping, membranes were blocked and incubated with primary antibodies as described above. After washing, membranes were incubated with HRP-conjugated secondary antibody diluted 1:10000 in 1% BSA in TBS-T for 2 h at RT, washed four times, and bands were revealed as previously described.

Adjusted density for each band was calculated using Image J software and density signals were normalized compared to loading control signal and/or corresponding total protein levels. Primary Antibodies: phospho-ERK1/2$^{T202:Y204}$ (Cell Signaling Technology, #4370), phospho-SAPK/JNK$^{T183:Y185}$ (Cell Signaling Technology, #4668), and mouse anti-$\alpha$tubulin as loading control (Sigma Aldrich, #T6199). Secondary antibodies: HRP-conjugated polyclonal goat anti-rabbit IgG (Dako, #P0448) and HRP-conjugated polyclonal goat anti-mouse IgG (Dako, #P0447).

*Statistical Analysis*: All data (without previous modification) are presented as mean ± standard error of the mean (SEM). One-way and two-way analysis of variance (ANOVA) and Tukey and Bonferroni *post hoc* tests were applied to calculate the differences between the values. Values of $p < 0.05$ were considered statistically significant. All statistical analysis was performed using the Prism 9.5 software.

## Supporting Information

Supporting Information is available from the Wiley Online Library or from the author.

## Acknowledgements

This work was supported by project CNS2022-135700 funded by MICIU/AEI /10.13039/501100011033 and the European Union NextGenerationEU/PRTR and by funding from the European Research Council (ERC) under the European Union's Horizon 2020 research and innovation programme (grant agreement No 853468). S.D.S.F. is the recipient of a Marie Skłodowska-Curie Postdoctoral Fellowship (HORIZON-MSCA-2021-PF-01-01, Grant agreement No 101064735) funded by the European Union. AC.F-L acknowledges financial support thanks to the DGA predoctoral fellowship 2023–2027. C.T acknowledges financial support under the

National Recovery and Resilience Plan (NRRP), Mission 4, Component 2, Investment 1.1, Call for tender No. 1409 published on 14.9.2022 by the Italian Ministry of University and Research (MUR), funded by the European Union – NextGenerationEU– Phoenix: Enhancing tissue regeneration through carbon nanoheaters, CUP B53D23031710001, Grant Assignment Decree No. 1369 adopted on 01/09/2023 by the Italian Ministry of Ministry of University and Research (MUR). The authors would like to acknowledge Fondo Social del Gobierno de Aragón (grupo DGA E15_23R), the use of Advanced Microscopy Laboratory (Universidad de Zaragoza) for access to their instrumentation and expertise, and the use of the Servicio General de Apoyo a la Investigación-SAI, Universidad de Zaragoza.

## Conflict of Interest

The authors declare no conflict of interest.

## Author Contributions

G.T. and S.D.S.F. contributed equally to this work and are the first co-authors. G.T. performed the investigation (experiments with *Hydra*), data curation, formal analysis, and writing draft. S.D.S.-F. performed the investigation (synthesis, functionalization, and characterization of MNPs, regeneration assays), data curation, formal analysis, and writing (draft, review, and editing). A.C.F.-L. performed the investigation (western blot analysis, evaluation of the catalytic properties of MNPs), and formal analysis. A.L. performed the investigation (FRAP, thiol levels, catalase activity, lipid peroxidation assay), writing (review). M.W. performed the investigation (FRAP, thiol levels, catalase activity, lipid peroxidation assay), writing (review). C.T. developed the research concept and methodology and reviewed the final draft. M.M. acquired funds, developed research concepts, methodology, and prepared the original draft preparation, reviewed and edited the final draft.

## Data Availability Statement

The data that support the findings of this study are available from the corresponding author upon reasonable request.

## Keywords

*Hydra vulgaris*, magnetic hyperthermia, magnetic nanoparticles, ROS, tissue regeneration

Received: March 27, 2024
Revised: June 14, 2024
Published online:

[1] A. van der Vliet, Y. M. W. Janssen-Heininger, *J. Cell. Biochem.* **2014**, *115*, 427.
[2] G. Wang, F. Yang, W. Zhou, N. Xiao, M. Luo, Z. Tang, *Biomed. Pharmacother.* **2023**, *157*, 114004.
[3] N. Bryan, H. Ahswin, N. Smart, Y. Bayon, S. Wohlert, J. Hunt, *Eur Cell Mater* **2012**, *24*, 249.
[4] T. Finkel, *J. Cell Biol.* **2011**, *194*, 7.
[5] C. Gauron, C. Rampon, M. Bouzaffour, E. Ipendey, J. Teillon, M. Volovitch, S. Vriz, *Sci. Rep.* **2013**, *3*, 2084.
[6] N. R. Love, Y. Chen, S. Ishibashi, P. Kritsiligkou, R. Lea, Y. Koh, J. L. Gallop, K. Dorey, E. Amaya, *Nat. Cell Biol.* **2013**, *15*, 222.
[7] E. Gracia-Latorre, L. Pérez, M. Muzzopappa, M. Milán, *Nat. Commun.* **2022**, *13*, 4794.
[8] E. Tur, L. Bolton, B. E. Constantine, *J. Am. Acad. Dermatol.* **1995**, *33*, 217.
[9] A. E. K. Loo, Y. T. Wong, R. Ho, M. Wasser, T. Du, W. T. Ng, B. Halliwell, *PLoS One* **2012**, *7*, e49215.
[10] H. Sies, D. P. Jones, *Nat. Rev. Mol. Cell Biol.* **2020**, *21*, 363.
[11] G. Onorato, F. Fardella, A. Lewinska, F. Gobbo, G. Tommasini, M. Wnuk, A. Tino, M. Moros, M. R. Antognazza, C. Tortiglione, *Adv. Healthcare Mater.* **2022**, *11*, 2200366.
[12] M. Moros, A. Lewinska, G. Onorato, M. R. Antognazza, F. Di Maria, M. Blasio, G. Lanzani, A. Tino, M. Wnuk, C. Tortiglione, *MRS Commun.* **2018**, *8*, 918.
[13] K. Khorsandi, R. Hosseinzadeh, H. Esfahani, K. Zandsalimi, F. K. Shahidi, H. Abrahamse, *Inflamm. Regen.* **2022**, *42*, 40.
[14] M. Migliario, P. Yerra, S. Gino, M. Sabbatini, F. Renò, *Antioxidants* **2023**, *12*, 1550.
[15] E. Carrasco, M. I. Calvo, A. Blázquez-Castro, D. Vecchio, A. Zamarrón, I. J. D. De Almeida, J. C. Stockert, M. R. Hamblin, Á. Juarranz, J. Espada, *J. Invest. Dermatol.* **2015**, *135*, 2611.
[16] S. del Sol-Fernández, P. Martínez-Vicente, P. Gomollón-Zueco, C. Castro-Hinojosa, L. Gutiérrez, R. M. Fratila, M. Moros, *Nanoscale* **2022**, *14*, 2091.
[17] H. Gavilán, S. K. Avugadda, T. Fernández-Cabada, N. Soni, M. Cassani, B. T. Mai, R. Chantrell, T. Pellegrino, *Chem. Soc. Rev.* **2021**, *50*, 11614.
[18] J. T. Dias, M. Moros, P. Del Pino, S. Rivera, V. Grazú, J. M. De La Fuente, *Angew. Chem. Int. Ed.* **2013**, *52*, 11428.
[19] M. Moros, A. Ambrosone, G. Stepien, F. Fabozzi, V. Marchesano, A. Castaldi, A. Tino, J. M. De La Fuente, C. Tortiglione, *Nanomedicine* **2015**, *10*, 2167.
[20] S. W. Flanagan, P. L. Moseley, G. R. Buettner, *FEBS Lett.* **1998**, *431*, 285.
[21] I. Belhadj Slimen, T. Najar, A. Ghram, H. Dabbebi, M. Ben Mrad, M. Abdrabbah, *Int. J. Hyperthermia* **2014**, *30*, 513.
[22] R. J. Wydra, P. G. Rychahou, B. M. Evers, K. W. Anderson, T. D. Dziubla, J. Z. Hilt, *Acta Biomater.* **2015**, *25*, 284.
[23] A. Sola-Leyva, Y. Jabalera, M. A. Chico-Lozano, M. P. Carrasco-Jiménez, G. R. Iglesias, C. Jimenez-Lopez, *J. Mater. Chem. B* **2020**, *8*, 7667.
[24] C. Pucci, A. Degl'Innocenti, M. Belenli Gümüş, G. Ciofani, *Biomater. Sci.* **2022**, *10*, 2103.
[25] R. J. Wydra, C. E. Oliver, K. W. Anderson, T. D. Dziubla, J. Z. Hilt, *RSC Adv.* **2015**, *5*, 18888.
[26] B. Hobmayer, M. Jenewein, D. Eder, M. K. Eder, S. Glasauer, S. Gufler, M. Hartl, A. W. Salvenmoser, *Int. J. Dev. Biol.* **2012**, *56*, 509.
[27] A. Gierer, S. Berking, H. Bode, C. N. David, K. Flick, G. Hansmann, H. Schaller, E. Trenkner, *Nat New Biol* **1972**, *239*, 98.
[28] H. Watanabe, V. T. Hoang, R. Mättner, T. W. Holstein, *Semin. Cell Dev. Biol.* **2009**, *20*, 1114.
[29] M. Moros, L. Gonzalez-Moragas, A. Tino, A. Laromaine, C. Tortiglione, *Nanomaterials for Magnetic and Optical Hyperthermia Applications* (Eds. R. M. Fratila, J. M. de la Fuente), Elsevier, Amsterdam, The Netherlands, **2019**, pp. 229.
[30] M. Moros, A. Lewinska, F. Merola, P. Ferraro, M. Wnuk, A. Tino, C. Tortiglione, *ACS Appl. Mater. Interfaces* **2020**, *12*, 13718.
[31] A. Ambrosone, P. del Pino, V. Marchesano, W. J. Parak, J. M. de la Fuente, C. Tortiglione, *Nanomedicine* **2014**, *9*, 2829.
[32] G. Veronesi, M. Moros, H. Castillo-Michel, L. Mattera, G. Onorato, K. D. Wegner, W. L. Ling, P. Reiss, C. Tortiglione, *ACS Appl. Mater. Interfaces* **2019**, *11*, 35630.
[33] M. Allocca, L. Mattera, A. Bauduin, B. Miedziak, M. Moros, L. De Trizio, A. Tino, P. Reiss, A. Ambrosone, C. Tortiglione, *Environ. Sci. Technol.* **2019**, *53*, 3938.

[34] S. Del Sol Fernández, O. F. Odio, P. M. Crespo, E. O. Pérez, G. Salas, L. Gutiérrez, M. P. del Morales, E. Reguera, *J. Phys. Chem. C* **2022**, *126*, 10110.
[35] S. D. Oberdick, A. Abdelgawad, C. Moya, S. Mesbahi-Vasey, D. Kepaptsoglou, V. K. Lazarov, R. F. L. Evans, D. Meilak, E. Skoropata, J. van Lierop, I. Hunt-Isaak, H. Pan, Y. Ijiri, K. L. Krycka, J. A. Borchers, S. A. Majetich, *Sci. Rep.* **2018**, *8*, 3425.
[36] M. Moros, B. Hernáez, E. Garet, J. T. Dias, B. Sáez, V. Grazu, A. González-Fernández, C. Alonso, J. M. De La Fuente, *ACS Nano* **2012**, *6*, 1565.
[37] M. Moros, B. Pelaz, P. López-Larrubia, M. L. García-Martin, V. Grazú, J. M. de la Fuente, *Nanoscale* **2010**, *2*, 1746.
[38] C. Castro-Hinojosa, S. Del Sol-Fernández, E. Moreno-Antolín, B. Martín-Gracia, J. G. Ovejero, J. M. de la Fuente, V. Grazú, R. M. Fratila, M. Moros, *Bioconjug Chem* **2023**, *34*, 2275.
[39] E. Amiruddin, A. Awaluddin, S. Sinuraya, H. Hadianto, M. D. Noferdi, A. S. Fitri, *J. Phys. Conf. Ser.* **2021**, *2049*, 012021.
[40] J. Kim, H. R. Cho, H. Jeon, D. Kim, C. Song, N. Lee, S. H. Choi, T. Hyeon, *J. Am. Chem. Soc.* **2017**, *139*, 10992.
[41] T. Valdés-Solís, P. Valle-Vigón, S. Álvarez, G. Marbán, A. B. Fuertes, *Catal. Commun.* **2007**, *8*, 2037.
[42] A. C. M. Maldonado, E. L. Winkler, M. Raineri, A. T. Córdova, L. M. Rodríguez, H. E. Troiani, M. L. M. Pisciotti, M. V. Mansilla, D. Tobia, M. S. Nadal, T. E. Torres, E. De Biasi, C. A. Ramos, G. F. Goya, R. D. Zysler, E. Lima, *J. Phys. Chem. C* **2019**, *123*, 20617.
[43] N. Daviu, Y. Portilla, M. Gómez de Cedrón, A. Ramírez de Molina, D. F. Barber, *Biomaterials* **2024**, *304*, 122409.
[44] B. Quinn, F. Gagné, C. Blaise, *Int. J. Dev. Biol.* **2012**, *56*, 613.
[45] A. Ambrosone, C. Tortiglione, *Toxicol. Mech. Methods* **2013**, *23*, 207.
[46] O. K. Wilby, J. M. Tesh, *Toxicol. In Vitro* **1990**, *4*, 582.
[47] R. Schaible, F. Ringelhan, B. H. Kramer, T. Miethe, *Exp. Gerontol.* **2011**, *46*, 794.
[48] V. Marchesano, Y. Hernandez, W. Salvenmoser, A. Ambrosone, A. Tino, B. Hobmayer, J. M. de la Fuente, C. Tortiglione, *ACS Nano* **2013**, *7*, 2431.
[49] T. D. Skokan, B. Hobmayer, K. L. McKinley, R. D. Vale, *Mol. Biol. Cell* **2024**, *35*.
[50] C. Dunnill, T. Patton, J. Brennan, J. Barrett, M. Dryden, J. Cooke, D. Leaper, N. T. Georgopoulos, *Int. Wound J.* **2017**, *14*, 89.
[51] D. Bridge, A. G. Theofiles, R. L. Holler, E. Marcinkevicius, R. E. Steele, D. E. Martínez, *PLoS One* **2010**, *5*, e11686.
[52] L.-O. Klotz, C. Sánchez-Ramos, I. Prieto-Arroyo, P. Urbánek, H. Steinbrenner, M. Monsalve, *Redox Biol.* **2015**, *6*, 51.
[53] R. Liang, S. Ghaffari, *Curr. Top. Dev. Biol.* **2018**, *127*, 23.
[54] A.-M. Boehm, K. Khalturin, F. Anton-Erxleben, G. Hemmrich, U. C. Klostermeier, J. A. Lopez-Quintero, H.-H. Oberg, M. Puchert, P. Rosenstiel, J. Wittlieb, T. C. G. Bosch, *Proc. Natl. Acad. Sci. USA* **2012**, *109*, 19697.
[55] C. R. Reczek, N. S. Chandel, *Curr. Opin. Cell Biol.* **2015**, *33*, 8.
[56] Y. Nakamura, C. D. Tsiairis, S. Özbek, T. W. Holstein, *Proc. Natl. Acad. Sci. USA* **2011**, *108*, 9137.
[57] M. C. Vogg, B. Galliot, C. D. Tsiairis, *Development* **2019**, *146*, dev177212.
[58] J. F. Cazet, A. Cho, C. E. Juliano, *elife* **2021**, *10*, 60562.
[59] H. O. Petersen, S. K. Höger, M. Looso, T. Lengfeld, A. Kuhn, U. Warnken, C. Nishimiya-Fujisawa, M. Schnölzer, M. Krüger, S. Özbek, O. Simakov, T. W. Holstein, *Mol. Biol. Evol.* **2015**, *32*, 1928.
[60] B. Hobmayer, F. Rentzsch, K. Kuhn, C. M. Happel, C. C. von Laue, P. Snyder, U. Rothbächer, T. W. Holstein, *Nature* **2000**, *407*, 186.
[61] G. A. Haval, K. D. Pekhale, N. A. Perween, S. M. Ghaskadbi, S. S. Ghaskadbi, *J. Biochem. Mol. Toxicol.* **2020**, *34*, e22577.
[62] R. Murad, A. Macias-Muñoz, A. Wong, X. Ma, A. Mortazavi, *Genome Biol. Evol.* **2021**, *13*, evab221.
[63] M. C. Vogg, L. Beccari, L. Iglesias Ollé, C. Rampon, S. Vriz, C. Perruchoud, Y. Wenger, B. Galliot, *Nat. Commun.* **2019**, *10*, 312.
[64] R. Suzuki, T. Hiraiwa, A. Tursch, S. Höger, K. Hayashi, S. Özbek, T. W. Holstein, M. Tanaka, *bioRxiv* **2023**, 558226.
[65] N. Suknovic, S. Reiter-Karam, O. Chara, W. Buzgariu, D. Martinvalet, B. Galliot, *bioRxiv* **2022**, 510867.
[66] A. Tursch, N. Bartsch, M. Mercker, J. Schlüter, M. Lommel, A. Marciniak-Czochra, S. Özbek, T. W. Holstein, *Proc. Natl. Acad. Sci. USA* **2022**, *119*, 2204122119.
[67] Y. Wang, R. Branicky, A. Noë, S. Hekimi, *J. Cell Biol.* **2018**, *217*, 1915.
[68] B. Dash, R. Metz, H. J. Huebner, W. Porter, T. D. Phillips, *Gene* **2006**, *381*, 1.
[69] A. N. Bashkatov, E. A. Genina, V. I. Kochubey, V. V. Tuchin, *J. Phys. D Appl. Phys.* **2005**, *38*, 2543.
[70] L. Wang, P. Hu, H. Jiang, J. Zhao, J. Tang, D. Jiang, J. Wang, J. Shi, W. Jia, *Nano Today* **2022**, *43*, 101401.
[71] L. Li, X. Zhang, J. Zhou, L. Zhang, J. Xue, W. Tao, *Small* **2022**, *18*, 2107705.
[72] M. A. Voinov, J. O. S. Pagán, E. Morrison, T. I. Smirnova, A. I. Smirnov, *J. Am. Chem. Soc.* **2011**, *133*, 35.
[73] S. Fu, S. Wang, X. Zhang, A. Qi, Z. Liu, X. Yu, C. Chen, L. Li, *Colloids Surf B Biointerfaces* **2017**, *154*, 239.
[74] Z. Chen, J.-J. Yin, Y.-T. Zhou, Y. Zhang, L. Song, M. Song, S. Hu, N. Gu, *ACS Nano* **2012**, *6*, 4001.
[75] J. Jay-Gerin, *Biochimie* **2000**, *82*, 161.
[76] M. Colasanti, V. Mazzone, L. Mancinelli, S. Leone, G. Venturini, *Nitric Oxide* **2009**, *21*, 164.
[77] J. Zielonka, M. Zielonka, A. Sikora, J. Adamus, J. Joseph, M. Hardy, O. Ouari, B. P. Dranka, B. Kalyanaraman, *J. Biol. Chem.* **2012**, *287*, 2984.
[78] D. Dębski, R. Smulik, J. Zielonka, B. Michałowski, M. Jakubowska, K. Dębowska, J. Adamus, A. Marcinek, B. Kalyanaraman, A. Sikora, *Free Radic. Biol. Med.* **2016**, *95*, 323.
[79] K. Aquilano, S. Baldelli, M. R. Ciriolo, *Front. Pharmacol.* **2014**, *5*, 196.
[80] S. Baldelli, F. Ciccarone, D. Limongi, P. Checconi, A. T. Palamara, M. R. Ciriolo, *Nutrients* **2019**, *11*, 2318.
[81] H. Zeng, P. M. Rice, S. X. Wang, S. Sun, *J. Am. Chem. Soc.* **2004**, *126*, 11458.
[82] C. Gruttner, K. Muller, J. Teller, *IEEE Trans. Magn.* **2013**, *49*, 177.
[83] W. F. Loomis, H. M. Lenhoff, *J. Exp. Zool.* **1956**, *132*, 555.
[84] A. Ambrosone, L. Mattera, V. Marchesano, A. Quarta, A. S. Susha, A. Tino, A. L. Rogach, C. Tortiglione, *Biomaterials* **2012**, *33*, 1991.
[85] T. C. G. Bosch, C. N. David, *Dev. Biol.* **1984**, *104*, 161.
[86] K. J. Livak, T. D. Schmittgen, *Methods* **2001**, *25*, 402.